Hindawi Publishing Corporation
Advances in Optical Technologies
Volume 2016, Article ID 5757361, 12 pages
http://dx.doi.org/10.1155/2016/5757361

Research Article

Quartz Enhanced Photoacoustic Spectroscopy for Detection of Improvised Explosive Devices and Precursors

Roberto Viola, Nicola Liberatore, Domenico Luciani, and Sandro Mengali

Consorzio CREO (Centro Ricerche Elettro Ottiche), SS.17 Località Boschetto, 67100 L'Aquila, Italy

Correspondence should be addressed to Roberto Viola; roberto.viola@consorziocreo.it

Received 2 September 2015; Revised 23 December 2015; Accepted 28 December 2015

Academic Editor: Partha P. Banerjee

A compact portable and standalone point sensor has been developed for the detection and identification of precursors of improvised explosive devices (IEDs) and to be part of a network of sensors for the discovery of hidden bomb factories in homeland security applications. The sensor is based on quartz enhanced photoacoustic spectroscopy (QEPAS), and it implements a broadly tunable external cavity quantum cascade laser source (EC-QCL). It makes use of an optical cell purposely designed with a miniaturized internal volume, to achieve fast response and high sensitivity, and that can also be heated to improve sensitivity towards less volatile compounds. The sensor has been assembled and successfully tested in the lab with several compounds, including IED's precursors such as acetone, nitromethane, nitric acid, and hydrogen peroxide. The identification capability and limits of detection near the ppm level have been estimated for all these compounds.

1. Introduction

The discovery of hidden bomb factories is of primary importance in the prevention of terrorist activities. In the early stages of IED preparation for a terrorist attack, investigations can be conducted with less time constraints and with greater accuracy than at later stages. Beyond the use of audio and video monitoring, an interesting approach to localize the factory is through the detection of the precursors that are released around the site while they are manipulated and transformed into the final IEDs. A number of precursors have been identified which need to be addressed as a matter of priority. The detection of explosives and precursors and more research into enhancing detectability prior to explosion have been explicitly stated as a priority by the Commission of European Communities [1].

Requirements imply that the sensors should be operated locally in distributed networks and that data gathered by such networks should be evaluated by expert operators. Such monitoring activities are necessary to alert counter terrorism units sufficiently in advance of a planned terrorist action.

The work presented in this paper deals with the development of a *point sensor* for the detection and identification of traces of precursors, in the *vapour phase,* used in IED production [2]. This sensor is based on Quartz Enhanced Photo Acoustic Spectroscopy (QEPAS) [3], which is one of the many forms of infrared absorption spectroscopy, particularly interesting for allowing the extremely small size and reduced costs of its analysis cell. While QEPAS sensors generally operate in a narrow spectral window around the sharp absorption peak of a given small-mass molecule [4–11], our sensor uses a widely tunable laser source to scan a vast portion of the spectrum, to detect and recognize the fingerprints of a number of relatively complex molecules with broad absorption patterns. A few examples of this approach are reported in the literature [12–15]. Also our QEPAS cell implements heating elements and microfluidic connections with minimized dead volumes, which make the sensor arranged for hyphenation with sampling, preconcentration, and micro-Gas Chromatographic separation modules. This configuration is expected to exploit at the best the miniaturized volume of the cell and enable analysis of complex vapour mixes with increased sensitivity and faster response. Finally, our sensor is designed to be remotely operated as a node of a wireless network.

This work was mainly devoted to the description of the sensor. Results from early lab measurements have been also included, in order to demonstrate its detection

and identification capabilities, with a suitable sensitivity, towards a limited set of compounds of interest. Different scenarios were analyzed, and a few common characteristics were identified that need to be taken into account in the definition of requirements and in the design of the system, which is, essentially as follows:

(1) *The range of chemical targets is wide*. The sensor should be able to detect and identify a number of precursors, corresponding to different IEDs.

(2) *Events of interests may have a rapid time evolution* (in the order of minutes or even seconds); this is due to the fact that (a) the sensor might cross through a localized gas cloud on board of a car at nonnegligible speed; (b) gas clouds might be released only occasionally and towards directions depending on variable weather conditions when precursors are brought to reaction.

(3) *Concentration of target gases may be low*. IEDs' concentration in the vapour phase will be a fraction of the saturation concentration. Even for precursors with high vapour pressure, the concentration can decrease rapidly when the gas cloud spreads out of the bomb factory location. Detection limit of the system should be appreciably lower than the saturation concentration of targeted vapours.

(4) *Interfering compounds could be present*. They may mask the signals of the target, thus decreasing the Probability of Detection (PoD); or they may mimic the signals of the target, thus increasing the Probability of False Alarm (PFA). The system and its pattern recognition algorithms should be able to reject signals from interfering compounds.

(5) *Background fluctuations are a source of noise*. Even when assuming to compensate thermal fluctuation of the background, nasty forms of noise could arise from fluctuations of the concentration of common air components in the timescale of the measurement. The system should be able to reject signals due to background fluctuations.

2. Materials and Methods

Starting from a relatively long list of reported IED's precursors, we focused our study on the compounds that feature strong absorption bands in the spectral range of our laser source. They are listed in Table 1.

Most of them are liquid or even solid at normal ambient conditions and their standard vapour pressures span over several orders of magnitude: from a few ppm of less volatile compounds (e.g., hexamine) to tens of thousands of ppm of much more volatile compounds (e.g., acetone). For hexamine and DNT, vapours tend to condense at cold surfaces while travelling through the sensor, which makes quantitative analysis controversial without accurate sensor thermalization at high temperature. Consequently, in this work, just some preliminary results are reported for hexamine and DNT, and we limit the discussion to the results that were obtained for acetone, nitromethane, nitric acid 68% in water, and hydrogen peroxide 33% in water. All these chemicals are available as standard products from Panreac.

Table 1: IED's precursors tested with the QEPAS sensor.

Common name	State	Vapour pressure (mmHg@20°C)
Acetone	Liquid	184
Hydrogen peroxide	Liquid	2
Nitric acid	Liquid	48
Hexamine	Solid	<0.01
DNT	Solid	<0.001
Nitromethane	Liquid	28

Several tests were arranged in the lab to verify detection and identification capability of the sensor. Also quantitative tests to evaluate limits of detection (LoDs) were performed, by sampling controlled mixtures. A schematic of the experimental set-up for these tests is depicted in Figure 1.

A sealed canister, with an internal volume of 6 liters, was utilized as an evaporation chamber filled with nitrogen at ambient pressure. Initially, while the by-pass was open and the input and output valves of the canister were closed, controlled amounts of liquid were injected inside through the septum, by means of a microsyringe. Due to the small amount of liquid injected (a few microliters), the max vapour concentration inside the canister was determined assuming complete vaporization of the liquid. Then, the resulting gas-vapour mix was pushed through the QEPAS optical cell by opening the input and output valves and by closing the by-pass.

We used the microsyringe in our lab tests to have easier and reliable control of the quantities of compounds used. For real and stand-alone operation of the sensor, the air is sampled directly inside the QEPAS cell by means of a micropump.

2.1. QEPAS Sensor Overview. The QEPAS technique, early described by Kosterev et al. [3], is a quite new approach to detect weak photoacoustic signals in a gas medium. In a QEPAS experiment, a laser beam is focused between the prongs of a quartz tuning fork (QTF) and its intensity or, alternatively, its wavelength is modulated at the resonant frequency of the tuning fork. When the small air volume between the prongs contains a gas that absorbs the laser radiation, acoustic waves are generated that induce the oscillation of the tuning fork. The QTF converts these mechanical oscillations into an electrical output signal that can be demodulated by a lock-in amplifier system. The demodulated signal is proportional to the concentration of the gas, its absorption coefficient, the optical power of the laser, and the quality factor of the oscillator and inversely proportional to the resonant frequency [16]. Furthermore, absorption spectra can be recorded by scanning the laser wavelength [11, 15]. The architecture of our QEPAS sensor is illustrated in Figure 2.

In our sensor, the QTF is mounted inside a μL size stainless steel chamber and coupled to the external laser by means

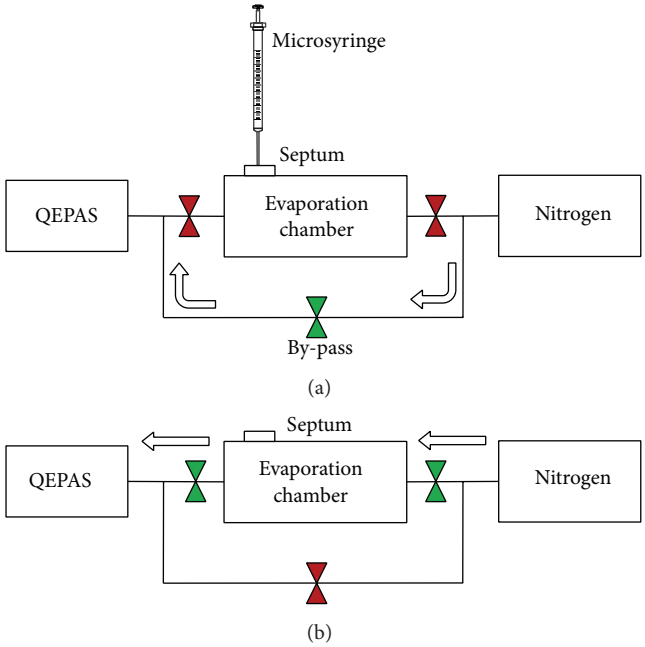

Figure 1: Schematics of the experimental set-up. (a) The liquid is injected inside the evaporation chamber, the input and output valves are closed, and the nitrogen can flow through the by-pass; (b) the input and output valves are opened, the by-pass is closed, and the vapours flow through the QEPAS.

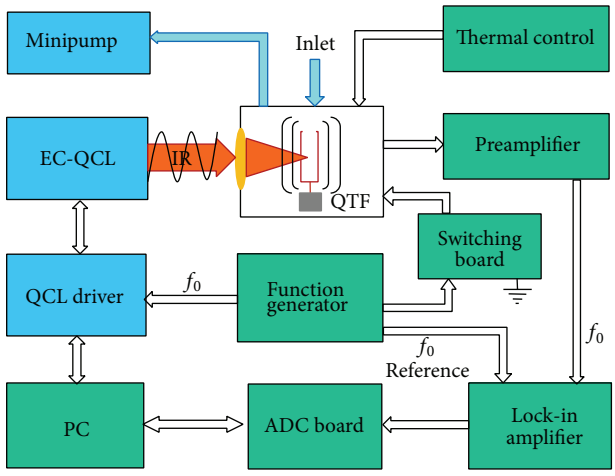

Figure 2: Architecture of the QEPAS sensor.

of refractive optics. A custom-designed hardware machine interface (HMI), running on a local PC controller, allows us to manage the sensor operation and the data acquisition. The HMI communicates with the laser controller to set its emission parameters. It also sets the acquisition parameter of the ADC board and receives digital data from it. Looking at Figure 2, the function generator triggers the pulsed emission of the laser and provides the reference signal to the lock-in amplifier, which demodulates the output signal from the preamplifier of the QTF, before sending it to the ADC board. The auxiliary thermal control allows us to operate the QEPAS above room temperature, when dealing with low volatility

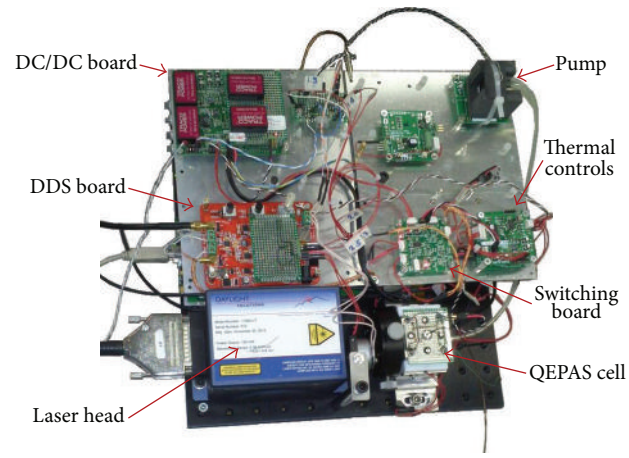

Figure 3: Compact breadboard of the QEPAS sensor head showing the laser head and the optical cell assembled and some of the electronic boards implemented. All the electronics, including the lock-in board, the preamplifier, and the ADC board, were assembled, though they are not visible in the picture, since being hidden under the metallic plates.

precursors, to increase concentration of vapours and avoid strong recondensation inside the QEPAS cell. The minipump was used for direct air sampling to draw the vapours inside the QEPAS cell through a small inlet aperture. It has been subsequently substituted by a vapour preconcentration unit (VPC) to improve the sensor performance. The switching board allows us to switch from the measurement mode (the photoacoustic signal is read out) to the calibration mode (a modulated bias is applied to the QTF). The focusing lens focalized the laser beam between the two prongs of the QTF, and an acoustic microresonator (not shown in Figure 2) was implemented to intensify the photoacoustic wave, thus improving sensitivity.

In Figure 3, it is shown that a breadboard of the QEPAS sensor head developed.

Aiming at a compact and portable device to be easily deployable on the field, the laser head and the main optical and electronic components were assembled together on a common base plate of 300 mm × 300 mm. For the sake of robustness (installation on board of moving vehicles is foreseen), no moving part was implemented inside the QEPAS cell, which hosts the QTF and the microresonator. This will minimize the possible optical misalignment due to mechanical shocks. Finally the design was oriented to the selection of COTS (commercially off the shelf) optic and electronic components, when available, in order to contain costs for the development of the sensor head.

2.2. QCL Laser Head. To generate IR radiation pulses at the resonant frequency of the quartz tuning fork, in the useful MIR spectral range, and also considering the constrains on size and power consumption, a quantum cascade laser [17] was selected. A review of this type of laser is given by Capasso [18]. The choice of the QCL took into account of the spectral position of the IR fingerprints of the targeted IED's precursors. Furthermore, the spectral region below 7 μm

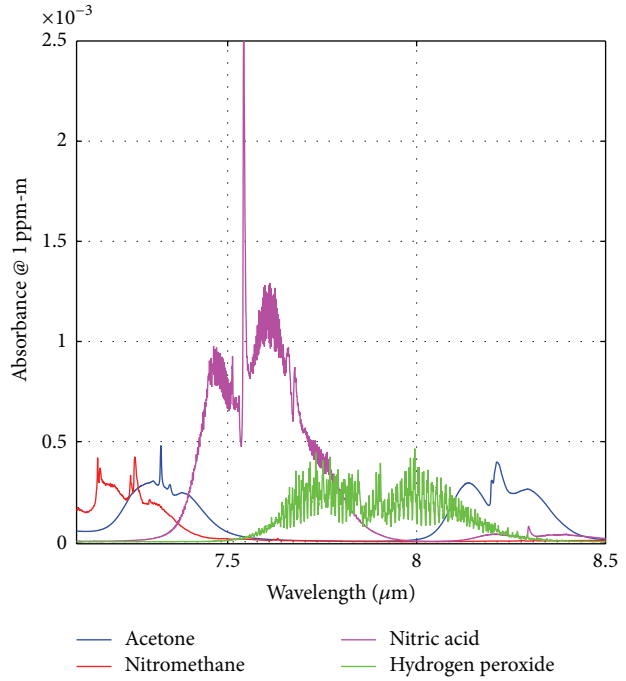

Figure 4: Absorption spectral fingerprint of four IED's precursors, as reported in the legend, in the working range of the UT8 laser source of our sensor.

was avoided, because the presence of water absorption could mask the targets. As a trade-off solution, we chose the UT8 source from daylight solutions. It is a broadly tunable EC-QCL, with pulsed emission up to the maximum allowed pulse repetition frequency (PRF) of 100 kHz. The laser line width is 1 MHz FWHM. It implements an external cavity tuning scheme and combines high emitted power (>400 mW at the pulse peak) with a wide spectral range, between 7.1 μm and 8.5 μm, which very well matches important features of many target compounds. Figure 4 shows the absorption spectra of four among the most interesting targets that were used in our laboratory tests, in the spectral range covered by the UT8.

A compact electronic board model IEMP V1.1 was implemented as a function generator to trigger the laser emission. It is an open-source simple DDS (Direct Digital Synthesis) board. It is a signal generator, based on Arduino environment, the AD9833 (a programmable waveform generator), and the AD603 (variable gain high frequency amplifier), providing sine/triangle/square waveform with frequency range from 100 Hz to 5 MHz. The laser was operated in pulse mode at the PRF corresponding to the actual resonance frequency of the QTF, which is updated automatically at the start of each measurement by means of a customized calibration board. At the nominal frequency of 32.768 kHz and at the maximum pulse duration of 500 ns, it corresponds to a duty cycle of less than 2%.

2.3. Laser Focusing Lens. The laser beam emitted by the EC-QCL source has a diameter of about 2.5 mm and a divergence of 5 mrad. In the QEPAS sensor, it must be focused within the two prongs of the quartz tuning fork. The gap between

Table 2: Specifications of the QTF.

Size	6 mm × 1.5 mm × 0.6 mm
Nominal frequency	32.768 kHz
Frequency tolerance	±20 ppm at 25°C
Operating temperature range	−10°C to +60°C
Load capacitance:	12.5 pF
ESR	35 kΩ
Shunt capacitance	0.85 pF
Motional capacitance	2.0 fF

the two prongs of the tuning fork is of about 300 μm; thus an IR focusing lens was needed. Simulations with the prescription data of COTS lenses have been carried out with the ZEMAX optical design program. The result was that a ZnSe plano convex singlet of 12.7 mm diameter and 25 mm focal length could be suitable to obtain appropriate focusing of the laser with simple and compact optical configuration (avoiding more complex and costly multiple elements assemblies). In addition, the quite short focal length of the selected lens allowed minimizing the size of the optical cell and of the head of the sensor as a whole. A fine positioning mount allowed the fine alignment of the focused laser beam between the two prongs of the QTF. For the sake of the robustness and reliability of the QEPAS sensor, this positioning mount was the only moveable part of the optomechanical assembly.

2.4. Quartz Tuning Fork Resonator. The choice of the QTF was driven by the following constraints: (a) the interrogation volume should be minimized (when vaporizing solid/liquid particles, the smaller the interrogation volume is, the larger the concentration of the vapours and the response of the sensor are); (b) the distance between the prongs must be larger than the laser spot. These considerations lead to choose a small COTS QTF with a distance between the prongs of 300 μm. It is cheap and commercially available quartz tuning fork, which is commonly used in wristwatches. It is sold packaged in vacuum to resonate around 32.768 kHz. This type of quartz tuning fork has been utilized in most of the QEPAS sensors reported in the literature. Basic consideration about the QTF noise and about its quality factor Q and time response, at different experimental conditions, has been duly reported in previous works (see e.g., [4] and Kosterev et al. [15, 16]). The main characteristics of the QTF we used are reported in Table 2.

We extracted the QTF from its vacuum enclosure and fixed it inside our QEPAS cell in air. It is worth noting that although the selected QTF was specified by the manufacturer to work up to 60°C, its utilization in our QEPAS sensor was successfully tested up to 150°C. Possible implementation of this QTF at even higher temperature, for detection of low volatility compounds, has to be further explored.

2.5. Calibration of the Resonance Frequency. The QTF has to be excited at its resonance frequency to achieve the highest sensitivity. Due to the change in the environmental characteristics (specially temperature changes), the resonance frequency of the QTF drifts and the system

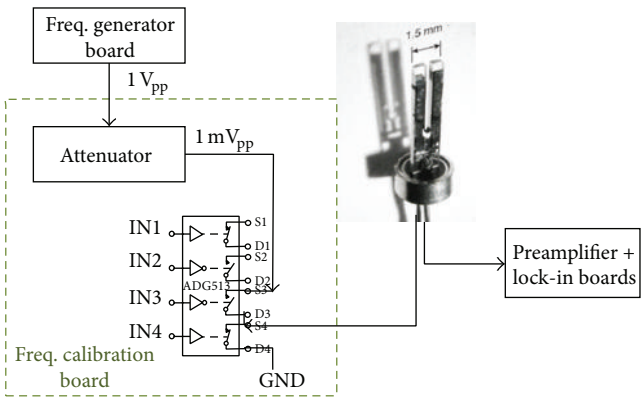

Figure 5: Scheme of the electronics for the calibration of the resonance frequency.

(e.g., the pulse repetition frequency of the QCL) needs to be calibrated. To apply the calibration, the sensor switches from the measurement mode (the photoacoustic signal is read out) to the calibration mode (a modulated bias is applied to the QTF). According to the frequency calibration scheme depicted in Figure 5, in the calibration phase one pin of the QTF is disconnected automatically (by means of a frequency calibration board) from GND and is connected with the attenuated sinusoidal output from a frequency generator board (the DDS board). Then, starting from a frequency below the nominal resonance of the QTF, this modulated bias is tuned across a range of frequencies and the response curve of the QTF is acquired. The resonance frequency is found by searching for the maximum of the response curve. Then, the pulse repetition frequency of the laser is set to the updated resonance frequency by means of the same DDS board, and the sensor is switched back from the calibration mode to the measurement mode. The whole calibration routine lasts for a few seconds. Electronics and SW routines were developed and implemented to apply a systematic run time calibration of the QTF. The calibration can be activated, before starting each measurement, to fix the actual resonance frequency of the QTF.

2.6. Acoustic Microresonator. An acoustic microresonator was manufactured and applied to amplify the photoacoustic wave and thus improve the sensitivity of the QEPAS sensor. The microresonator did consist of two small tubes of appropriate size that were positioned very close to the tuning fork. The length of the microresonator should be nearly equal to the path traveled by the acoustic wave in the period of time which corresponds to the resonance frequency of the QTF. Several microresonator tubes were manufactured, starting from stainless steel needles of different size and following design specifications from the literature [19, 20]. A set of microresonator tubes is shown in Figure 6. A representative layout of the microresonator and the corresponding device as assembled inside our QEPAS cell are also illustrated in Figure 6. The technical specifications of the selected microresonator are reported in Table 3.

Table 3: Technical specifications of the microresonator.

Material	Stainless steel
Internal diameter	0.5 mm
External diameter	0.8 mm
Length	4.6 mm
Distance from the QTF	<50 μm

2.7. Optical Cell. The optical cell hosts the QTF and the microresonator. It is an air-tight stainless steel cell with two small apertures to suck samples by means of an external mini pump. It also has an infrared optical window to allow the focused laser beam to enter the cell and propagate through the gap between the two prongs of the QTF. A layout of the design of the optical cell and a picture of the cell assembled are shown in Figure 7. The assembled cell is a cube of 4 cm size, with a useful internal volume of less than 100 μL.

Since detection of low volatility compounds can only proceed through thermal desorption of small amounts of liquids or solids, the internal volume of the optical cell was designed to be as small as possible, to maximize the concentration of desorbed vapours for a given amount of solid/liquid sample. The cell can be heated to avoid recondensation of vapours inside.

2.8. Electronics. The scheme of the electronics is depicted in Figure 8, in which the main connections between the several functional blocks are shown, except for the laser unit that had its own controller. The laser controller (not shown) was connected to the DDS (Direct Digital Synthesis) board, which generates both the trigger for the laser and the reference modulated signal for the lock-in, at the resonant frequency of the QTF. The interface board with the quartz tuning fork (QTF I/F board) is the same frequency calibration board illustrated in Figure 5. The GPS module was inserted for georeferencing of the sensor after deployment.

The ultralow noise current preamplifier, model LCA-200K-20M by FEMTO, was used to amplify the weak output signal of the QTF. It has 40 fA/$\sqrt{\text{Hz}}$ of equivalent input noise current, a transimpedance gain of 2×10^7 V/A, and a bandwidth from DC to 200 kHz. The preamplifier was inserted upstream of the dual phase lock-in amplifier model LIA-BVD-150-H by FEMTO. It is specified for a working frequency from 50 Hz to 120 kHz, voltage input range from 3 μV to 1 V, and voltage input noise of 12 nV/$\sqrt{\text{Hz}}$. The time constant was settable in the range from 300 μs to 1 s. Considering the full wavelength scan duration of about 4 seconds, we selected a time constant of 10 ms, as a trade-off between a time constant higher, to achieve a better S/N, and a time constant lower, to improve the spectral resolution of the QEPAS spectra. Although the X, Y, and R components were all available from the lock-in board, we chose to acquire only the R component, in order both to simplify and speed up the data processing and to avoid the need of adjusting the phase in our standalone and unattended sensor.

For AD conversion of the output signal from the lock-in amplifier, we used a COTS multichannel multifunction

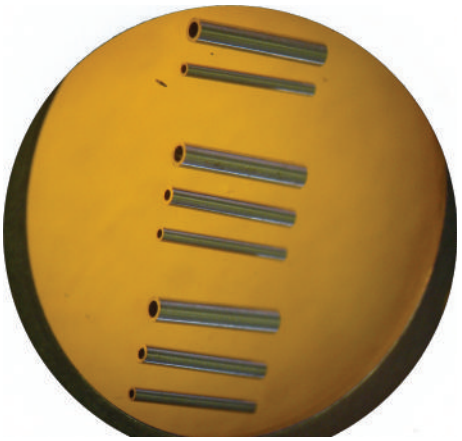

(a)

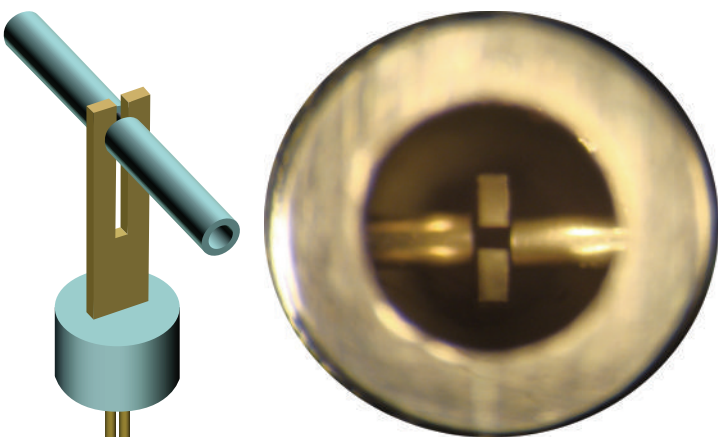

(b)

Figure 6: (a) a micrograph of a set of microresonator tubes manufactured by cutting and polishing of stainless steel needles. (b, left) A representative layout of the QTF and microresonator assembly; (b, right) a micrograph of the microresonator assembled very close to the QTF inside the optical cell of our QEPAS sensor.

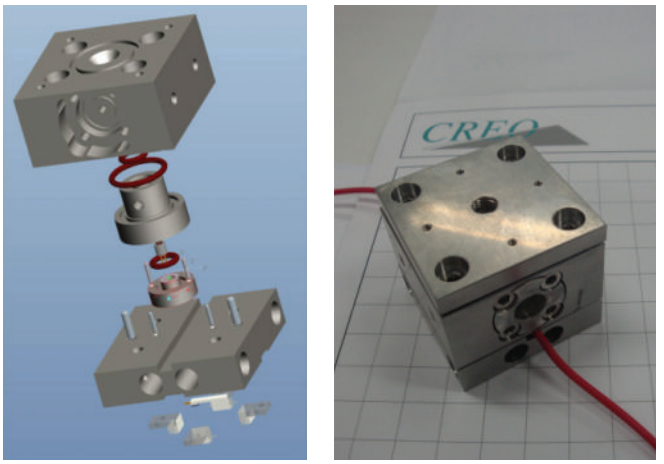

(a) (b)

Figure 7: Optical cell: exploded view of the cell design (a) and picture of the optical cell assembled, also showing the top lid for interfacing with a sampling unit (b).

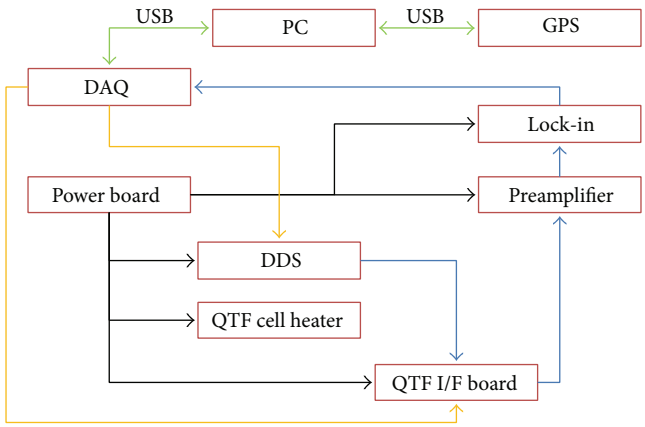

Figure 8: Scheme of the connections between the functional blocks of the electronics (color online): power supply lines (black arrows); digital signal/control lines (orange arrows); analog signal lines (light blue arrows); standard USB connections (green arrows).

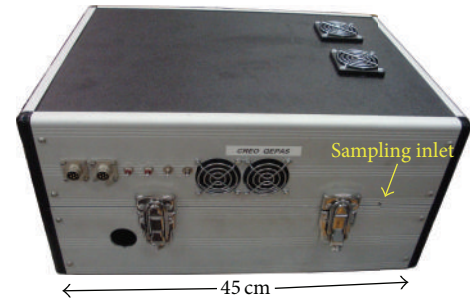

Figure 9: Picture of the whole QEPAS sensor packaged inside a small suitcase of 45 cm × 35 cm × 25 cm.

data acquisition (DAQ) device: the NI USB-6212 by National Instruments.

A purposely designed power board was developed. It was able to generate, with a input of 24 V, all the needed voltages for the boards into the QEPAS sensor.

It was designed with two stages: in the first stage, the switching regulators converted the input 24 V into a ±15 V, with efficiency higher than 80%, in order to reduce the power loss and the thermal heating; in the second stage, the linear regulators, with low dropout technology, reduced and stabilized the voltages, minimizing the noise and the output voltage ripple. The main components used in the switching regulators were the TRACO TEN series modules. They have an efficiency up to 86%, with isolation of 1500 V_{dc} and a shielded metal case (to minimize noise coupling). The main components for the linear regulators are the Linear Technologies LT3028 (for positive voltages) and LT1175 (for negative voltages): they have a dropout, (the minimum difference between input and output), of only 300 mV (this means lower power dissipation into the regulator), and they are able to provide up to 500 mA with extremely low noise (20 μV_{rms} for the LT3028).

Aiming to attain standalone and remote operation, lithium batteries were implemented to provide around 100 W to the laser controller and to supply all the other electronics of the sensor head with means of the power control board.

In order to operate our QEPAS unit with a network of sensors for the discovery of hidden bomb factories, the software interface (HMI) of the QEPAS sensor was developed to be run from a remote command center (CC), allowing us to manage the sensor remotely by means of a wireless transmission network based on TCP/IP. In our laboratory tests, a notebook was equipped with operative system Windows XP, to communicate locally with the optical head and manage the sensor by means of the same HMI. Custom software was also installed for the preprocessing of the signal acquired, in order to retrieve and save the QEPAS spectra. The same notebook was put inside the sensor suitcase together with a transmission node, for operating the sensor as a remote standalone unit. An IP address can be assigned to the sensor and data corresponding to the spectra acquired and preprocessed locally can be transferred from the sensor to the remote CC. The whole sensor package, of the size of an hand luggage, including also the laser controller and all the fluidics necessary for direct sampling of air, was assembled inside the small box shown in Figure 9.

3. Results and Discussion

The sensor was conceived to sample and measure continuously and cyclically air from the surrounding environment. When the sensor starts a measurement cycle, the first sample is treated as background and its spectrum subtracted from all subsequent measurements. Qualitative tests with several volatile IED's precursors dispersed in ambient air, in particular acetone, nitromethane, nitric acid, and hydrogen peroxide, were carried out successfully demonstrating a good identification capability of the corresponding absorption spectra. Pure nitrogen was used as a carrier gas for quantitative tests with controlled mixes of vapours, as illustrated in Figure 1. We used nitrogen, especially for quantitative measurements at fixed wavelength, to be sure that the variation of the photoacoustic signal was anyway only due to the absorption from the compound under test. We obtained very similar results when using dry air. We made also measurements with ambient air. The main effect of water vapour in the air sample is some signal fluctuation at wavelengths corresponding to water absorption lines. It is well known that large fluctuations of water vapour can severely affect the response of the sensor [21, 22], since they produce a shift in the resonance frequency of the tuning fork and can influence the photoacoustic relaxation processes. In our case, the problem is mitigated by calibrating the resonance frequency of the QTF automatically at each new measurement cycle. In the course of the cycle, which lasts only a few minutes, it is realistic to assume constant average water vapour concentration.

A sensitivity below the ppm level was obtained, even though some issues arose with nitric acid and hydrogen peroxide, due to the high chemical reactivity of such compounds.

Nevertheless, our main objective was to achieve fast response combined with identification ability against a broad range of chemicals. The system uses an External Cavity QCL

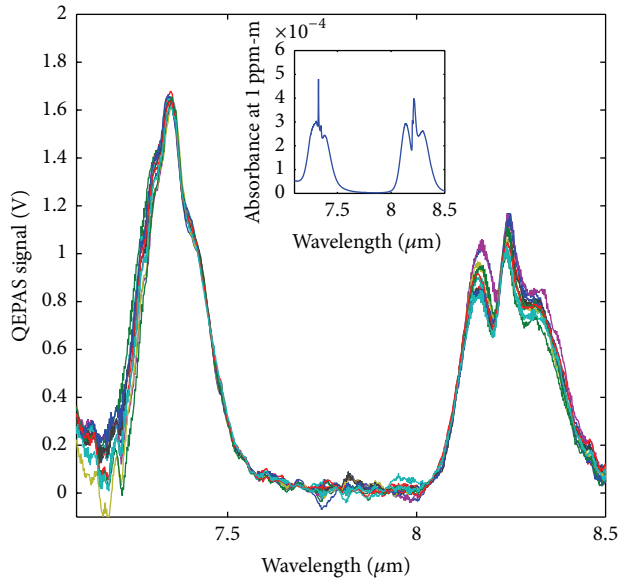

Figure 10: Absorption spectra of 200 ppm of acetone obtained with our QEPAS sensor (multicolor plots). The corresponding high resolution spectrum of 1 ppm acetone from the PNNL database is also shown for reference (in the inset).

to scan a spectral window of about 250 cm^{-1} at a frequency of about 0.5 Hz. Individual spectra are generated and processed at each new scan. When the composition of the air sample starts to change, new absorption patterns emerge. Averaging over a sequence of spectra is possible but implies longer response time.

In Figures 10, 12, 14, and 16, the reference spectra and the spectral response of our sensor to 200 ppm of each one of the selected precursors are reported. In these plots, the contribution of the background signal has been subtracted, in order to extract the absorption features of the sampled target. The background contribution has been estimated by means of measurements operated just before the sampling of the target chemicals. These plots give visual evidence, of the spectral identification capability of the sensor. Similar measurements were performed at lower concentrations down to a few ppm. Even though the S/N of the corresponding spectral response was poorer, it was possible to retrieve the target identification by means of standard techniques of data processing and classification, based on principal component analysis. In any case, we were more interested in demonstrating identification abilities rather than extreme sensitivity.

Other sets of measurements were carried out with a lock-in time constant of 1 second, at fixed wavelength corresponding to the absorption peak of the target compounds. If we assume that the minimum measurable concentration corresponds to a signal variation equal to the standard deviation of the background signal, the LoD associated with the reported plot can be calculated by dividing the concentration of the sample used for the test, by the value of the signal to noise ratio of the corresponding signal acquired while the sample flowed through the QEPAS cell. The values of the parameters derived from reported measurements and utilized to calculate

Table 4: Limits of detection.

Compound	C_0 (ppm)	σ (mV)	ΔS (V)	LoD (ppb)
Acetone	190	1.26	2.18	110
Nitromethane	7	3.3	0.09	257
Nitric acid	200	2.55	1.05	486
H_2O_2	200	2.64	0.89	593

the estimates of LoDs are reported in Table 4, where C_0 is the vapour concentration sampled from the evaporation chamber; σ is the standard deviation of the background signal (acquired before switching on the sample); ΔS is the signal measured while the sample passed through the QEPAS cell; LoD is the corresponding limit of detection, calculated as $\text{LoD} = C_0/(\Delta S/\sigma)$.

It is worth noting that although the noise level remains rather constant in all the four experiments, we obtained higher LoDs for nitric acid and hydrogen peroxide, with respect to the acetone. Since the absorption cross sections of hydrogen peroxide and nitric acid, at the selected wavelengths, are comparable to or even higher than acetone, we argue that the real concentration of hydrogen peroxide and nitric acid inside the QEPAS cell could be lower than inside the evaporation chamber, due to the interaction of reactive vapours with the transfer line. Although the LoDs reported in Table 4 are just an estimate, they indicate sensitivities that can match the requirements of an early warning sensor placed out of a bomb factory, particularly if the sensor is coupled with a simple sampling/preconcentration stage as discussed above.

3.1. Tests with Acetone. Figure 10 shows a sequence of infrared absorption spectra measured while 200 ppm of acetone in nitrogen was flushed through the optical cell. The high resolution absorption spectrum of 1 ppm of acetone, from the PNNL (Pacific Northwest National Laboratory) database [23], is also reported as an inset for reference. The spectral absorption bands of acetone were clearly identified, though QEPAS spectra exhibit a spectral resolution that did not allow us to resolve narrower peaks. This was due to the relatively slow response of the QTF with respect to the fast sweep of wavelengths (about 4 s for a complete wavelength scan). The multiple scan was reported to describe both the spectral resolutions achieved by the sensor for a single scan and also to show the repeatability of the measurement over several scans, during continuous monitoring of sampled air containing a fixed concentration of the target compound.

Figure 11 shows the response of the QEPAS sensor to 190 ppm of acetone at the peak absorption wavelength of 8217 nm. It was obtained by recording the QEPAS signal, while switching between fluxes of nitrogen and a mix at 190 ppm of acetone through the optical cell by means of the experimental set-up depicted in Figure 1.

A limit of detection of about 100 ppb was estimated for acetone from this result.

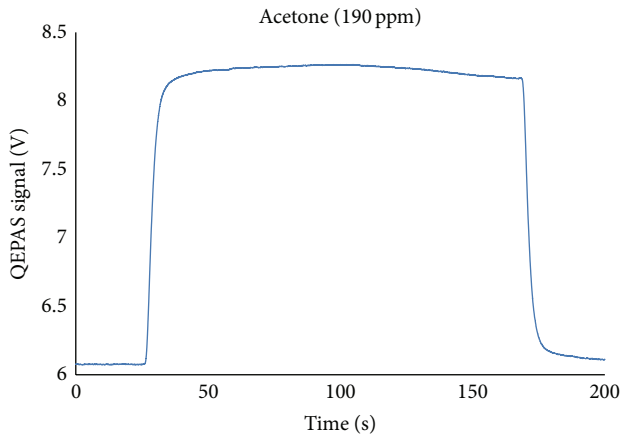

Figure 11: QEPAS response at the peak absorption wavelength of acetone at 8217 nm. The flux of a mix of acetone, at 190 ppm, was switched on at ca. 25 s and then switched off at ca. 170 s.

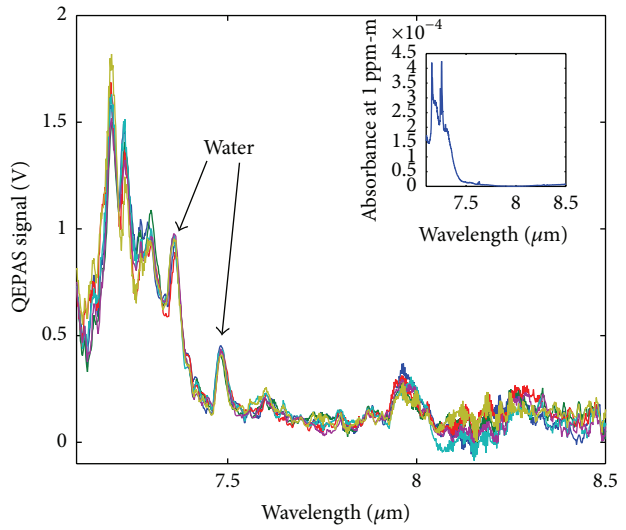

Figure 12: Absorption spectra of 200 ppm of nitromethane obtained with our QEPAS sensor (multicolor plots). Also peaks from water were clearly observed, since vapours were generated starting from a liquid mix of nitromethane and water. The high resolution spectrum of 1 ppm nitromethane from the PNNL database is also shown for reference (in the inset).

3.2. Tests with Nitromethane. Figure 12 shows a sequence of infrared absorption spectra measured while 200 ppm of nitromethane was flushed through the optical cell. To obtain the gas mixture at 200 ppm of nitromethane, a controlled amount of a liquid mix of nitromethane and water was previously evaporated and then flushed through the QEPAS optical cell. This explains the presence of the water absorption peaks in the measured spectra of Figure 12, where the absorption bands of both nitromethane and water were clearly identified.

Figure 13 shows the response of the QEPAS sensor to 7 ppm of nitromethane at the peak absorption wavelength of 7254 nm. It was obtained by switching between fluxes of air and of a mix at 7 ppm of nitromethane through the optical cell. To obtain this low concentrated vapour mix, we evaporated a liquid diluted solution at 1% of nitromethane in water. A limit of detection for nitromethane of about 260 ppb was estimated from these results.

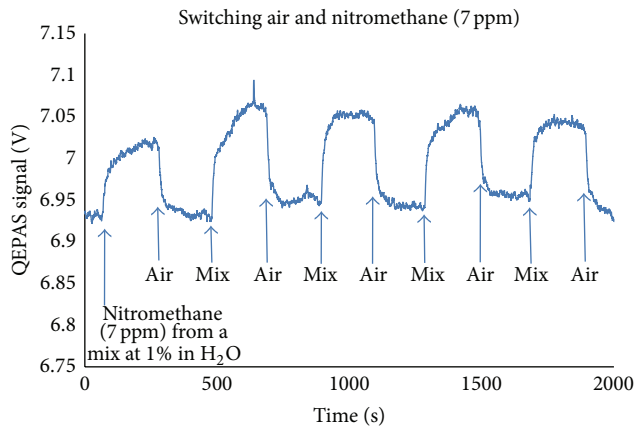

Figure 13: QEPAS response at the peak absorption wavelength of nitromethane at 7254 nm. The flux of a mix of nitromethane at 7 ppm and water vapour was switched on and off at several times, as indicated by the arrow in the plot. The QEPAS signal increased and decreased accordingly.

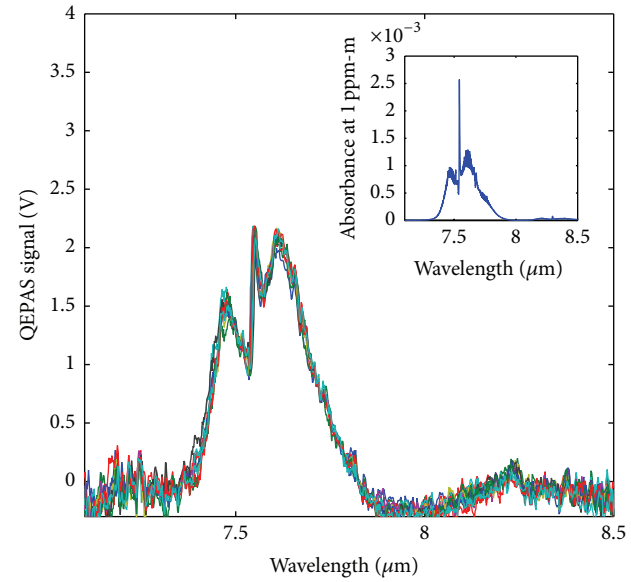

Figure 14: Absorption spectra of 200 ppm of nitric acid obtained with our QEPAS sensor (multicolor plots). The corresponding high resolution spectrum of 1 ppm nitric acid from the PNNL database is also shown for reference (in the inset).

3.3. Tests with Nitric Acid. In Figure 14, a sequence of infrared absorption spectra of 200 ppm of nitric acid measured by the QEPAS sensor is shown. To obtain the gas mixture at 200 ppm of nitric acid, a standard liquid nitric acid (68% in water) was utilized. Once again the spectral absorption bands of nitric acid were clearly identified, though narrower absorption peaks cannot be well resolved due to the fast scan sweep.

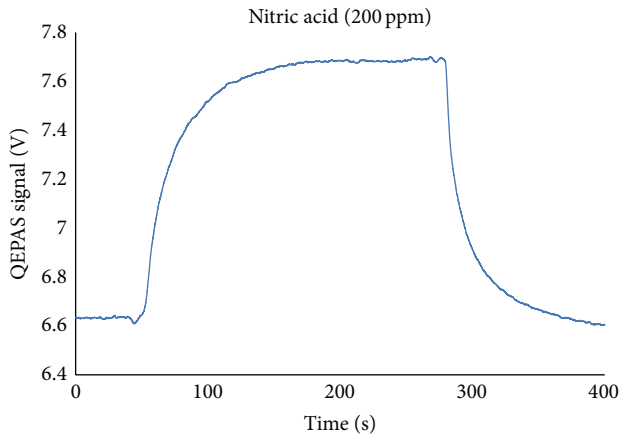

Figure 15: QEPAS response for nitric acid at the peak absorption wavelength of 7540 nm. The flux of a mix of nitric acid at 200 ppm was switched on at ca. 50 s and then switched off at ca. 280 s.

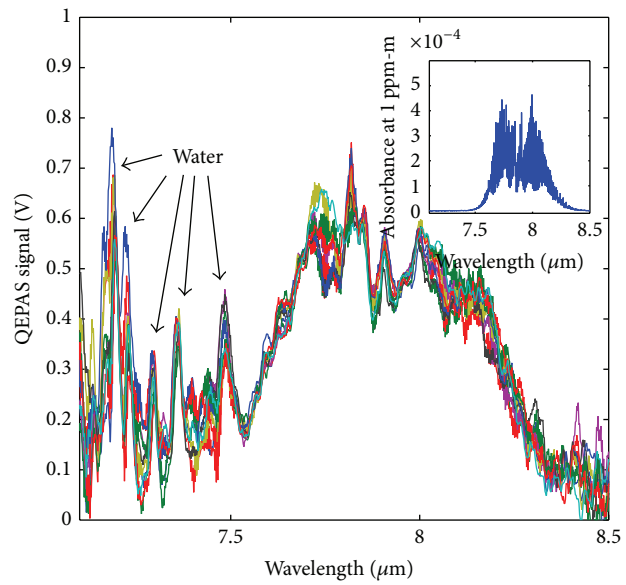

Figure 16: Absorption spectra of 200 ppm of hydrogen peroxide obtained with our QEPAS sensor (multicolor plots). Also several peaks from water were clearly observed, since vapours were generated starting from a liquid solution at 33% hydrogen peroxide in water. The high resolution spectrum of 1 ppm hydrogen peroxide from the PNNL database is also shown for reference (in the inset).

In Figure 15, the response of the QEPAS sensor to 200 ppm of nitric acid at the peak absorption wavelength of 7540 nm is shown. It was obtained by switching between fluxes of nitrogen and of a mix at 200 ppm of nitric acid through the optical cell.

A limit of detection for the nitric acid of about 480 ppb can be estimated from these results, even though the nitric acid exhibits values of absorption cross section higher than acetone and nitromethane. But it is stressed that this LoD could be an underestimate of the real actual detection limit. In fact, since vapours of nitric acid are strongly reactive, their concentration was probably decreased along the transfer line from the evaporation chamber, where a controlled amount of liquid standard nitric acid at concentration of 68% was evaporated, up to the QEPAS cell.

3.4. Tests with Hydrogen Peroxide. Figure 16 shows a sequence of infrared absorption spectra measured while 200 ppm of hydrogen peroxide was flushed through the optical cell. To obtain the gas mixture at 200 ppm hydrogen peroxide in air, a controlled amount of a liquid solution at 33% hydrogen peroxide in water was injected inside the evaporation chamber. As for the experiments with nitromethane, this explains the presence of the water absorption peaks in the spectra reported in Figure 16.

In Figure 17, the response of the QEPAS sensor to 200 ppm of hydrogen peroxide at the absorption peak wavelength of 7992 nm is shown. It was obtained by switching between fluxes of nitrogen and of the mix at 200 ppm of hydrogen peroxide through the optical cell. A limit of detection for the hydrogen peroxide of about 590 ppb was estimated from these results. As for the nitric acid, this value is higher than expected, if considering that hydrogen peroxide has about the same peak absorption cross section of acetone and nitromethane. Also, in this case, the concentration was probably decreasing along the transfer line from the evaporation chamber to the QEPAS cell, due to the high chemical reactivity of hydrogen peroxide, and this limit of detection should be considered as an underestimate of the actual detection limit.

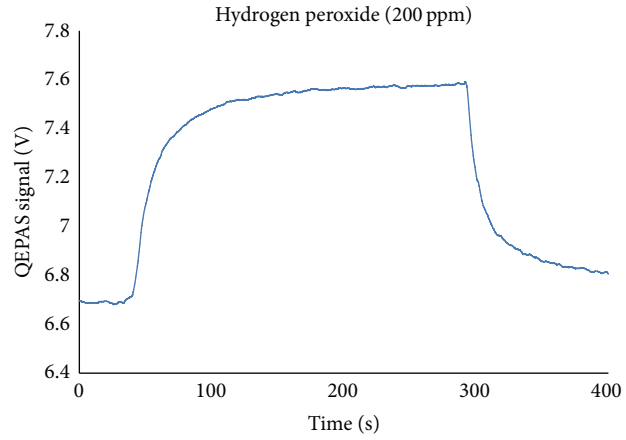

Figure 17: QEPAS response for hydrogen peroxide at the peak absorption wavelength of 7992 nm. The flux of a mix of hydrogen peroxide at 200 ppm was switched on at ca. 40 s and then switched off at ca. 290 s.

3.5. Test with Hexamine and DNT. These precursors are solid at normal ambient temperature and exhibit very low vapour pressure. The set-up illustrated in Figure 1 was proved unfit to analyze these substances. We tried to increase the concentration of vapours under test, by evaporating small amounts of solid over a hot plate and by increasing the temperature of the QEPAS optical cell up to 150°C, by means of the heating system and the thermal control implemented in the sensor. A small funnel was put on top of the hot plate

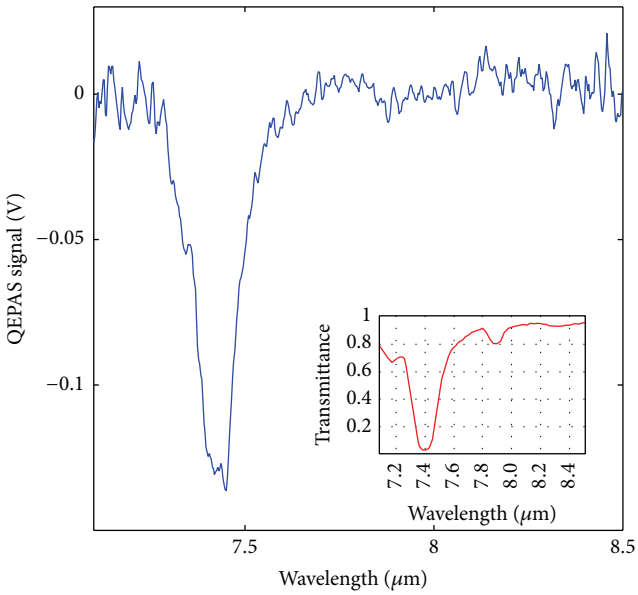

Figure 18: IR spectrum of DNT obtained with the QTF cell heated at 150°C (full plot) and comparison with the spectral transmittance of DNT from the database of NIST (in the inset).

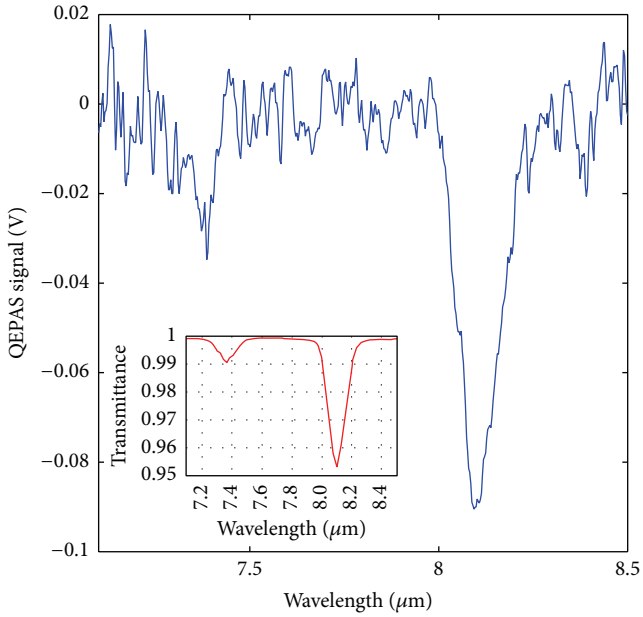

Figure 19: IR spectrum of hexamine obtained with the QTF cell heated at 150°C (full plot) and comparison with the spectral transmittance of hexamine from the database of NIST (in the inset).

and was connected to the sampling inlet of the sensor. The vapours were collected by means of the sampling minipump. The QEPAS spectra obtained for DNT and hexamine and the corresponding transmittance curves from the NIST database are shown in Figures 18 and 19, respectively. Also in these figures the background signal has been subtracted to obtain the plotted curves. The QEPAS spectra resemble those of DNT and hexamine, but the sign appears inverted (the QEPAS signal should increase in correspondence with the absorptions). Since we acquired the R component of the signal from the lock-in, we cannot explain this behavior with a phase shift of the QEPAS signal with respect to the background. We can infer that the QTF was still active at 150°C, giving anyway a positive identification of the sampled compounds. But, most likely, the concentration of vapours transferred inside the QEPAS cell was too high or even some recondensation took place, so that we observed the effect of direct absorption of the laser radiation, which reduced the QEPAS signal with respect to the background level. An improvement of the experimental set-up and additional testing will be needed to assess effectively the identification capability and LoDs of the sensor for these compounds.

4. Conclusion

A compact QEPAS sensor, the size of hand-luggage, has been designed and developed to be operated on the field as a part of a network of sensors for the discovery of hidden bomb factories. This sensor has been successfully assembled and tested in the lab, demonstrating both detection and identification capability towards a set of IED's precursors in the vapour phase. The implementation of a broadly tunable EC-QCL source allowed us to clearly identify, with a single source, the broad spectral absorption features of different IED's precursors in the midinfrared fingerprint spectral region. Also in our sensor new capabilities were implemented: (1) a QEPAS cell of miniature internal volume that allows us to be fast and also open the chance to hyphenate the sensor with preconcentration and GC separation units, by means of connections with minimized dead volumes, in order to improve both selectivity and sensitivity with trace amounts; (2) the possibility to work at high temperature to deal with low volatile compounds, also by means of connection with preconcentration and desorption units; (3) the optimization of the design and the implementation of batteries, in order to operate the sensor as a rugged portable standalone unit of compact size; (4) the implementation of wireless transmission to allow the utilization of the sensor as a part of a network of sensors remotely controlled. Altogether these peculiarities allow us to overcome some limitations of existing sensing approaches.

The absorption bands of tested compounds were clearly identified, by comparison with the reference database available from the PNNL. In particular, a sensitivity close to the ppm level was proven for acetone, nitromethane, nitric acid, and hydrogen peroxide, at fixed selected wavelengths corresponding to peaks of absorption and operating with a lock-in time constant of 1 second. Exploiting the possibility of heating the optical cell of our sensor up to 150°C, preliminary results, even with low volatile IED's precursors, such as hexamine and DNT, have been obtained. They indicated the sensor ability to identify their spectral absorption features, even though the need for some improvement has emerged to manage the sampling of heated vapours, such as an higher working temperature to avoid recondensation inside the optical cell. In our vision, the dramatic progress in QCLs and the parallel and analogous progress in silicon micromachining technology will enable the development

of highly integrated and miniaturized GC-QEPAS systems that, by exploiting the physical and chemical scaling laws of sensitivity and response speed, can compete with IMS and with GC/Mass instruments, not only in terms of costs, ruggedness, maintenance, and portability, but also in terms of sensing performance.

Further work is ongoing to assess the effective performance of the sensor in real environments. For this purpose, a database of experimental spectra of several compounds is under construction, including interferents and mixes. Furthermore, in the meanwhile, two validation campaigns on the field have been carried out. The description of updated outcomes and also of some upgrade of the hardware will be object of a forthcoming work.

Conflict of Interests

The authors declare that there is no conflict of interests regarding the publication of this paper.

Acknowledgment

The research leading to these results has received funding from the European Community's Seventh Framework Program (FP7-SEC-2010 N° 261685).

References

[1] Communication from the Commission to the European Parliament and the Council on Enhancing the Security of Explosives, http://ec.europa.eu/transparency/regdoc/rep/1/2007/EN/1-2007-651-EN-F1-1.Pdf.

[2] R. L. Woodfin, *Trace Chemical Sensing of Explosives*, John Wiley & Sons, New York, NY, USA, 2007.

[3] A. A. Kosterev, Y. A. Bakhirkin, R. F. Curl, and F. K. Tittel, "Quartz-enhanced photoacoustic spectroscopy," *Optics Letters*, vol. 27, no. 21, pp. 1902–1904, 2002.

[4] M. D. Wojcik, M. C. Phillips, B. D. Cannon, and M. S. Taubman, "Gas-phase photoacoustic sensor at 8.41 μm using quartz tuning forks and amplitude-modulated quantum cascade lasers," *Applied Physics B*, vol. 85, no. 2-3, pp. 307–313, 2006.

[5] M. Jahjah, S. Moumdji, O. Gauthier-Lafaye, S. Bonnefont, Y. Rouillard, and A. Vicet, "Antimonide-based 2.3 μm photonic crystal coupled-cavity lasers for CH_4," *Electronics Letters*, vol. 48, no. 5, pp. 277–278, 2012.

[6] M. Jahjah, S. Belahsene, L. Nähle et al., "Quartz enhanced photoacoustic spectroscopy with a 3.38 μm antimonide distributed feedback laser," *Optics Letters*, vol. 37, no. 13, pp. 2502–2504, 2012.

[7] K. Liu, X. Guo, H. Yi, W. Chen, W. Zhang, and X. Gao, "Off-beam quartz-enhanced photoacoustic spectroscopy," *Optics Letters*, vol. 34, no. 10, pp. 1594–1596, 2009.

[8] A. A. Kosterev, L. Dong, D. Thomazy, F. K. Tittel, and S. Overby, "QEPAS for chemical analysis of multi-component gas mixtures," *Applied Physics B: Lasers and Optics*, vol. 101, no. 3, pp. 649–659, 2010.

[9] V. Spagnolo, A. A. Kosterev, L. Dong, R. Lewicki, and F. K. Tittel, "NO trace gas sensor based on quartz-enhanced photoacoustic spectroscopy and external cavity quantum cascade laser," *Applied Physics B*, vol. 100, no. 1, pp. 125–130, 2010.

[10] V. Spagnolo, P. Patimisco, S. Borri, G. Scamarcio, B. E. Bernacki, and J. Kriesel, "Part-per-trillion level SF6 detection using a quartz enhanced photoacoustic spectroscopy-based sensor with single-mode fiber-coupled quantum cascade laser excitation," *Optics Letters*, vol. 37, no. 21, pp. 4461–4463, 2012.

[11] Y. Ma, R. Lewicki, M. Razeghi, and F. K. Tittel, "QEPAS based ppb-level detection of CO and N2O using a high power CW DFB-QCL," *Optics Express*, vol. 21, no. 1, pp. 1008–1019, 2013.

[12] R. Lewicki, G. Wysocki, A. A. Kosterev, and F. K. Tittel, "QEPAS based detection of broadband absorbing molecules using a widely tunable, cw quantum cascade laser at 8.4 μm," *Optics Express*, vol. 15, no. 12, pp. 7357–7366, 2007.

[13] M. C. Phillips, T. L. Myers, M. D. Wojcik, and B. D. Cannon, "External cavity quantum cascade laser for quartz tuning fork photoacoustic spectroscopy of broad absorption features," *Optics Letters*, vol. 32, no. 9, pp. 1177–1179, 2007.

[14] C. Bauer, U. Willer, R. Lewicki et al., "A mid-infrared QEPAS sensor device for TATP detection," *Journal of Physics: Conference Series*, vol. 157, no. 1, Article ID 012002, 2009.

[15] A. A. Kosterev, P. R. Buerki, L. Dong, M. Reed, T. Day, and F. K. Tittel, "QEPAS detector for rapid spectral measurements," *Applied Physics B*, vol. 100, no. 1, pp. 173–180, 2010.

[16] A. A. Kosterev, F. K. Tittel, D. V. Serebryakov, A. L. Malinovsky, and I. V. Morozov, "Applications of quartz tuning forks in spectroscopic gas sensing," *Review of Scientific Instruments*, vol. 76, Article ID 043105, 2005.

[17] J. Faist, F. Capasso, D. L. Sivco, C. Sirtori, A. L. Hutchinson, and A. Y. Cho, "Quantum cascade laser," *Science*, vol. 264, no. 5158, pp. 553–556, 1994.

[18] F. Capasso, "High-performance midinfrared quantum cascade lasers," *Optical Engineering*, vol. 49, no. 11, Article ID 111102, 2010.

[19] L. Dong, A. A. Kosterev, D. Thomazy, and F. K. Tittel, "QEPAS spectrophones: design, optimization, and performance," *Applied Physics B*, vol. 100, no. 3, pp. 627–635, 2010.

[20] P. Patimisco, G. Scamarcio, F. K. Tittel, and V. Spagnolo, "Quartz-enhanced photoacoustic spectroscopy: a review," *Sensors*, vol. 14, no. 4, pp. 6165–6206, 2014.

[21] A. A. Kosterev, T. S. Mosely, and F. K. Tittel, "Impact of humidity on quartz-enhanced photoacoustic spectroscopy based detection of HCN," *Applied Physics B*, vol. 85, no. 2-3, pp. 295–300, 2006.

[22] A. Veres, Z. Bozóki, Á. Mohácsi, M. Szakáll, and G. Szabó, "External cavity diode laser based photoacoustic detection of CO_2 at 1.43 μm: the effect of molecular relaxation," *Applied Spectroscopy*, vol. 57, no. 8, pp. 900–905, 2003.

[23] Pacific Northwest National Lab (PNNL) database of IR absorption spectra, https://secure2.pnl.gov/nsd/nsd.nsf/Welcome.